

A high-dimensional, stochastic model for twin-screw granulation

Part 2: Numerical methodology

Andrew D. McGuire^a, Sebastian Mosbach^a, Kok Foong Lee^a, Gavin Reynolds^b, Markus Kraft^{a,c,*}

^a*Department of Chemical Engineering and Biotechnology, University of Cambridge, Philippa Fawcett Dr, Cambridge, CB3 0AS, United Kingdom*

^b*Pharmaceutical Technology & Development, AstraZeneca, Charter Way, Macclesfield, SK10 2NA, United Kingdom*

^c*School of Chemical and Biomedical Engineering, Nanyang Technological University, 62 Nanyang Drive, Singapore 637459*

Abstract

In the second part of this study, we present the stochastic weighted particle population balance framework used to solve the twin-screw granulation model detailed in the first part of this study. Each stochastic jump process is presented in detail, including a new nucleation jump event capable of capturing the immersion nucleation processes in twin-screw granulation. A variable weighted inception algorithm is presented and demonstrated to reduce the computational cost of simulations by up to two orders of magnitude over traditional approaches. The relationship between the performance of the simulation algorithm and key numerical parameters within the nucleation jump process are explored and optimum operating conditions identified. Finally, convergence studies on the complete simulation algorithm demonstrate that the algorithm is very robust against changes in the number of stochastic particles used, provided that the number of particles exceeds a minimum required for numerical stability.

Keywords: granulation, twin-screw, stochastic particle model, population balance model, stochastic weighted algorithm

*Corresponding author
Email address: mk306@cam.ac.uk (Markus Kraft)

1. Introduction

In the first part of this study we introduced, optimised and investigated the qualitative behaviour of a four dimensional model for twin-screw granulation under various operating conditions. In this part of the study we are primarily concerned with presenting and investigating the properties of the numerical methods employed/developed to solve this high dimensional model and overcome the numerical challenges inherent to the stochastic modelling of twin-screw systems.

Granulation is the transformation of solid primary particles to agglomerate form. These agglomerates may have a size, porosity and liquid distribution that allow them to be utilised within the pharmaceutical and food industries, among others [1]. The granulation process is typically modelled mechanistically using population balance models (PBM) [2] (though non-mechanistic pure neural network approaches have also been investigated [3, 4]). Using PBMs, the particle ensemble is transformed through processes such as nucleation, coagulation, breakage, consolidation, layering and wetting.

In general, granulation PBMs are numerically solved using variations of the sectional method [5, 6, 7, 8]. Through the sectional method, each particle dimension (e.g. solid volume, liquid volume etc.) is mapped onto a discrete grid. This allows the model to be represented as a system of ordinary differential equations, which can be solved numerically. The dimensionality of these sectional PBMs generally ranges from one [8] to three [9, 6] and a lumped parameter technique is often employed to estimate additional particle properties (such as internal gas volume [5]). To capture spatial inhomogeneities in processing conditions within the equipment, granulation PBMs often represent the system as a network of well-mixed compartments [10, 8]. In recent years, PBMs have been coupled (both unidirectionally and bidirectionally) with other simulation frameworks, such as the Discrete Element Method (DEM) [11]. DEM is typically used to capture collision data and compartment residence times for use in the PBM(s) [12, 9, 13]. However, the high computational cost of DEM

simulations has, in cases, incentivised their replacement with artificial neural networks (ANN). Barrasso and co-workers [14, 15] demonstrated the use of an ANN (trained on DEM data) in PBM-ANN couplings. The resulting couplings have been shown to reduce the computational cost of solution by several orders of magnitude (over PBM-DEM couplings), whilst maintaining the ability to predict key DEM data.

Though sectional models for granulation have been successfully applied to numerous systems in the past [6, 8], the method itself has a number of key limitations. The first of these limitations is the upper bound placed on the dimensionality of the particle model. In sectional solvers, this limit arises as the number of equations to be solved rapidly increases with the addition of each additional dimension. It is generally agreed that at most three dimensions can be specified before the solution process becomes computationally unfeasible [5]. Though, four dimensional sectional models have been tested, they can take several days or even weeks to solve [16]. This bound on dimensionality ultimately limits the number of ways that the modelled particles can be characterised and therefore limits the complexity of the particle mechanisms that can be employed. The second limitation of the sectional approach is that the resolution of the model along any particular dimension is controlled by the grid employed. All the particle mass within the same grid section is treated identically, meaning that there is a finite number of particles types than can be represented.

An alternative method of solving population balance models is the Monte Carlo particle method (sometimes referred to as MC-PBM or stochastic PBM). MC-PBMs have been successfully applied to the simulation of high-shear batch granulation [17, 18, 19, 20, 21, 22, 23, 24, 25]; silica nano-particle synthesis [26]; combustion engine modelling [27, 28]; soot formation [29, 30]; aerosol wet scavenging [31] and more general coagulation processes [32]. Under this framework, a representative sample volume of the system is modelled using an ensemble of computational particles. One such implementation of the stochastic particle method is Direct Simulation Monte Carlo, also know as the Direct Simulation

Algorithm (DSA). In DSA, each computational particle represents a single physical particle in the ‘real’ system. Each computational particle has an associated particle vector x that is used to characterise the physical particle it represents. In the case of granulation, this particle description may include the solid volume, various states of liquid volume and internal gas volume.

MC-PBM ensembles are evolved in time through Markov jump events that may act on/transform one or more particles at a time. These jump events represent the various particle mechanisms such as coagulation, breakage etc. These processes can be numerically challenging under DSA since highly unbalanced coagulation-breakage rates can lead to the undesired depletion or accumulation of computational particles [24]. Another disadvantage of the DSA method is that a large number of computational particles and repetitions of the simulation are often required to achieve an accurate sampling of the solution, both of which come at the cost of increased CPU time and memory [33]. The stochastic weighted particle method (also called the Stochastic Weighted Algorithm (SWA)), originally proposed by Rjasanow and Wagner [34], has been developed to overcome a number of the limitations of the DSA method. In SWA each computational particle has an associated statistical weight w . Using a number based weighting scheme under SWA, the number of ‘real’ particles represented by each computational particle x is proportional to w , and the ensemble is represented as a collection of coordinates (x, w) . SWA analogues of various particle processes such as coagulation [35, 36, 37] and breakage [38, 25] have been developed. Using SWA these processes can be formulated such that they conserve the number of computational particles (through the transformations of weights). Examples of constant number SWA processes are the coagulation jump processes presented by Patterson et al. [39] and the breakage processes of Lee et al. [25]. Zhao and co-workers [40, 36, 41] have also presented a SWA scheme to dynamically control the number of computational particles that fall within predefined volume intervals. This is done through the periodic modification of the number of computational particles and statistical weights within each volume interval. This “shift” action acts to maintain statistical precision

across the full range of the distribution.

In this paper, we are primarily concerned with the solution of the twin-screw granulation model presented in the first part of this study. Twin-screw granulation is a continuous method of wet granulation. The system consists of two co-rotating screws which convey solid material along the screw barrel (Figure 1). Liquid binder is injected at some point along the barrel length, which combines with the solid material and, under the action of the screw induced shear forces, leads to the formation of granules. For a comprehensive overview of twin-screw granulation as a process, the reader is referred to the first part of this study.

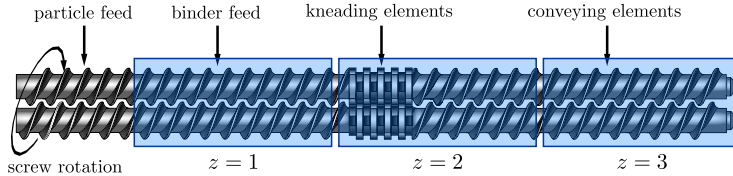


Figure 1: The TSG system with designated compartments as used in the first part of this study.

The modelling of TSG systems using SWA presents a number of inherent numerical difficulties. The first of these is the realisation of the immersion nucleation process that forms the preliminary agglomerates in the system. The liquid droplets that drive this nucleation process are much larger than the primary solid particles and their rate of inception is relatively low in comparison to processes such as particle collision. Nevertheless, this process is known to have a significant effect on the particle size distribution along length of the screw [42], necessitating the effective sampling of this jump process. Another key challenge in TSG modelling (and continuous granulation modelling in general) using stochastic PBMs is the continuous inception/removal of particles from a primary size distribution, since these distributions may encompass a volume range that extends over several orders of magnitude. Together, the set of algorithms used to address each of these particle process (and the other TSG

processes such as coagulation, breakage etc.) must be implemented in a manner that guarantees the fast solution of the model. This is essential for parameter estimation and large scale parametric sensitivity analysis, both of which can require thousands of model evaluations.

120 In this paper, we present the numerical framework used to solve the four-dimensional MC-PBM for twin-screw granulation (presented in the first part of this study) using the stochastic weighted particle method. The stochastic algorithm presented in this paper includes nucleation, inception, coagulation and fragmentation jump processes. A novel nucleation jump process is constructed,
125 which is capable of representing the multi-particle immersion nucleation processes in TSG systems. Further to this, we propose a new implementation of the SWA for the efficient initialisation/inception of particles from wide primary particle size distributions. A number of numerical studies are carried out to assess:

- 130 1. the relative performance of the newly proposed inception scheme;
2. the optimal choice of selected numerical parameters within the new nucleation jump process;
3. the general convergence properties of the algorithm in the context of the twin-screw granulation test case.

135 To the best of the authors' knowledge, this is the first time that a stochastic PBM has been applied to twin-screw granulation.

The remainder of the paper is structured as follows: in Section 2 the twin-screw granulation model is briefly detailed. The particle type-space and the formulation of each stochastic jump process is then detailed in Section 3. In
140 Section 4 we investigate potential algorithms for particle inception, the optimisation of key numerical parameters of the nucleation jump process and, finally, the convergence properties of the complete algorithm. The paper finishes with the presentation of the main findings of the work in Section 5.

2. Twin-screw granulation model

145 In this section we give a brief account of the twin-screw granulation model used in the numerical investigation. Only essential features are introduced for the propose of aiding readability. For an in-depth discussion of the model formulation the reader is directed to the first part of this study.

2.1. Particle type-space

150 In the twin-screw model, particles x are elements of the type-space \mathbb{X} and are described by a four-dimensional particle vector $x = (s_o, l_e, l_i, p)$ where: s_o is the volume of original solid, l_e is the volume of external liquid, l_i is the volume of internal liquid and p is the pore volume. The key derived particle properties are summarised in Table 1. Particles may take position in a bounded sequence

Table 1: Summary of derived particle properties. ρ_s and ρ_l are the solid and liquid densities, respectively.

Property	Nomenclature	Expression	Unit
Volume	$v(x)$	$s_o(x) + l_e(x) + p(x)$	m^3
Diameter	$d(x)$	$(6v(x)/\pi)^{1/3}$	m
Mass	$m(x)$	$\rho_s s_o(x) + \rho_l (l_i(x) + l_e(x))$	kg
Porosity	$\varepsilon(x)$	$p(x)/v(x)$	-

155 of compartments \mathbb{L} which forms a linear chain. Particles may flow between compartments and inter-particle processes are only permitted between particles in the same compartment $z \in \mathbb{L}$.

The possible particle processes (see Figure 2) are: nucleation, particle collision/compaction (which may or may not lead to coalescence), particle breakage, 160 particle transport (between compartments) and liquid penetration (where external liquid becomes internal liquid). The individual models for each of these processes is presented in the next section.

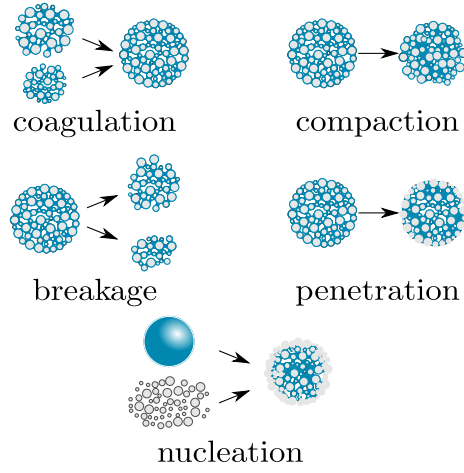


Figure 2: Particle processes in the TSG model presented in the first part of this study.

2.2. Inception/initialisation

In this model, particles with diameter d are incepted in the form of primary solid particles with the form

$$x_{\text{incept}} = (\pi d^3/6, 0, 0, 0), \quad (1)$$

This process occurs with rate

$$I_{\text{solid}}(z, dd) = \frac{\dot{M}_{\text{feed}} \mathbb{1}_{\{1\}}(z)}{\rho_s \bar{v}_{\text{incept}} V_{\text{real}}(z)} q_{0,\text{incept}}(d) dd, \quad (2)$$

where \dot{M}_{feed} is the mass feed rate to the real TSG system, $\mathbb{1}_{\mathcal{A}}$ is the indicator function on set \mathcal{A} , $q_{0,\text{incept}}(d)$ is the physical number distribution of particle diameters used for inception, $V_{\text{real}}(z)$ is the physical volume of compartment z and \bar{v}_{incept} is the arithmetic mean feed particle volume. This is given by

$$\bar{v}_{\text{incept}} = \int_{d_{\min}}^{d_{\max}} v(d) q_{0,\text{incept}}(d) dd, \quad (3)$$

where d_{\max} and d_{\min} are the maximum and minimum diameters of incepted particles, respectively.

In this paper, we assume that all real compartments have equal volume. Thus, if we have n_{comp} compartments and a total real system volume of $V_{\text{real,T}}$

then

$$V_{\text{real}}(z) = \frac{V_{\text{real,T}}}{n_{\text{comp}}}. \quad (4)$$

The feed distribution $q_{0,\text{incept}}$ used for inception and particle initialisation is taken from the volume fraction distribution presented in [43] for the Lactose Impalpable excipient grade. The diameter range is then split into 30 sections (spaced logarithmically). The discretised data is then converted into number distribution form $q_{0,\text{incept}}(d)$ using the relation [44]

$$q_{0,\text{incept}}(d) = \frac{q_3(d)d^{-3}}{\int_0^\infty q_3(d)d^{-3}dd}. \quad (5)$$

The total rate of inception events is then

$$R_{\text{incept}}(z, t) = \begin{cases} \dot{M}_{\text{feed}}/(\rho_s \bar{v}_{\text{incept}} V_{\text{real}}(z)) & \text{if } z = 1, \\ 0 & \text{otherwise} \end{cases}. \quad (6)$$

2.3. Liquid addition

Liquid droplets, consisting only of external liquid and with volume v_{drop} , are incepted into the first compartment with the form

$$x_{\text{drop}} = (0, v_{\text{drop}}, 0, 0). \quad (7)$$

Droplets are considered to be mono-disperse and the total rate of liquid addition events is

$$R_{\text{drop}}(z, t) = \begin{cases} \frac{(\text{LSR})\dot{M}_{\text{feed}}}{v_{\text{drop}}\rho_l V_{\text{real}}(z)}, & \text{if } z = 1, \\ 0, & \text{otherwise,} \end{cases} \quad (8)$$

where LSR and ρ_l are the liquid-solid mass feed ratio and liquid density, respectively.

170 2.4. Nuclei growth

In this work, nuclei growth is defined as the addition of particles to a droplet or semi-formed nuclei (a droplet which has acquired some degree of solid mass)

Hence, it is similar to a coagulation event, with the caveat that it involves a droplet/partially formed nucleus and another particle, which is not a droplet or partially formed nucleus. Further to this, immersion nucleation is defined as the process by which a droplet is incepted into the system, undergoes growth and produces a fully formed nucleus. The nuclei growth is described by the following particle size transformation:

$$x_{\text{nuc}}, x_i \mapsto T_{\text{nuc}}(x_{\text{nuc}}, x_i), \quad (9)$$

where $x_{\text{nuc}} \in \mathbb{X}_{\text{nuc}}, x_i \in \mathbb{X} \setminus \mathbb{X}_{\text{nuc}}$ (\mathbb{X}_{nuc} is the set of partially formed nuclei). The nucleation type-space transformation T_{nuc} is characterised by the individual property transformations:

$$s_{\text{o}}(T_{\text{nuc}}(x_{\text{nuc}}, x_i)) = s_{\text{o}}(x_{\text{nuc}}) + s_{\text{o}}(x_i) \quad (10)$$

$$l_{\text{e}}(T_{\text{nuc}}(x_{\text{nuc}}, x_i)) = l_{\text{e}}(x_{\text{nuc}}) \quad (11)$$

$$- \min([\phi_{\text{max}} - \phi(x_i)] \mathbb{1}_{\{x|\phi(x_i) \leq \phi_{\text{max}}\}}(x_i) s_{\text{o}}(x_i), l_{\text{e}}(x_{\text{nuc}})),$$

$$l_{\text{i}}(T_{\text{nuc}}(x_{\text{nuc}}, x_i)) = l_{\text{i}}(x_{\text{nuc}}) + l_{\text{i}}(x_i) + l_{\text{e}}(x_i) \quad (12)$$

$$+ \min([\phi_{\text{max}} - \phi(x_i)] \mathbb{1}_{\{x|\phi(x_i) \leq \phi_{\text{max}}\}}(x_i) s_{\text{o}}(x_i), l_{\text{e}}(x_{\text{nuc}})),$$

$$p(T_{\text{nuc}}(x_{\text{nuc}}, x_i)) = l_{\text{i}}(T_{\text{nuc}}(x_{\text{nuc}}, x_i)) / s^*, \quad (13)$$

where $\phi(x) = (l_{\text{i}} + l_{\text{e}}) / (s_{\text{o}})$ is the particle liquid saturation, ϕ_{max} is the maximum particle liquid saturation level permitted for the material of interest.

The nucleation kernel takes the form

$$K_{\text{nuc}}(x_{\text{nuc}}, x_i, z, t) = \begin{cases} k_{\text{nuc}}(z) \min(v(x_{\text{nuc}}), v(x_i)) & \text{if } \min(v(x_{\text{nuc}}), v(x_i)) < v_{\text{drop}}, \\ 0 & \text{otherwise,} \end{cases}$$

where k_{nuc} is the nucleation growth rate constant and since for the conditions we wish to model $v(x_{\text{nuc}}) > v(x_i) \forall i \in \{1, \dots, N(z, t)\}$, this can be simplified to

$$K_{\text{nuc}}(x_{\text{nuc}}, x_i, z, t) = \begin{cases} k_{\text{nuc}}(z) v(x_i) & \text{if } v(x_i) < v_{\text{drop}}, \\ 0 & \text{otherwise,} \end{cases} \quad (14)$$

The set of valid, completely formed nuclei is defined as $E = \{x \mid l_e(x) = 0\}$.

As noted by Hapgood et al. [45], with α -Lactose formulations and water
 175 binders, the droplet penetration time can likely be considered to be negligible.
 Hence, it is assumed that particle addition to the nuclei is instantaneous (i.e.
 $k_{\text{nuc}}(z) \rightarrow \infty \forall z \in \mathbb{L}$).

2.5. Coagulation

Particle collisions are modelled using a size-independent collision kernel given
 as

$$K_{\text{col}}(z, x_i, x_j) = n_{\text{screw}} k_{\text{col}}(z), \quad (15)$$

where n_{screw} is the operating screw speed and k_{col} is the collision rate constant
 180 in compartment z .

The Stokes criterion, as detailed in Braumann et al. [23], is used to determine
 whether or not a particular collision results in successful coalescence of the
 collision partners. Under this criterion, the probability of successful collision
 is dependent on the height of particle asperities H_a and particle coefficient of
 185 restitution e_{coag} .

2.6. Compaction

Each collision event leads to the compaction of the particles involved which
 reduces their porosity and squeezes liquid to particle surface. The compaction
 transform $T_{\text{comp}}(z, x)$ is characterised by the individual property transforms:

$$s_o \leftarrow s_o \quad (16)$$

$$l_e \leftarrow l_e + (T_{\text{comp}}^p(z, x) - p)l_i/p, \quad (17)$$

$$l_i \leftarrow l_i - (T_{\text{comp}}^p(z, x) - p)l_i/p, \quad (18)$$

$$p \leftarrow T_{\text{comp}}^p(z, x), \quad (19)$$

where

$$T_{\text{comp}}^p(z, x) = \frac{\varepsilon_1(z, x)(s_o + l_e + l_i)}{\varepsilon_1(z, x) \left(1 - \frac{l_i}{p}\right) - 1} \quad (20)$$

and

$$\varepsilon_1(z, x) = \begin{cases} k_{\text{comp}}(z)[\epsilon(x) - \epsilon_{\text{min}}] + \epsilon(x), & \text{if } \epsilon(x) \geq \epsilon_{\text{min}}, \\ \epsilon(x), & \text{otherwise.} \end{cases} \quad (21)$$

Here k_{comp} is the compaction rate constant, $\epsilon(x)$ is the particle porosity (as defined in Table 1) and ϵ_{min} is the minimum porosity permitted.

2.7. Breakage

In the TSG model, individual particles undergo binary breakage at rate

$$g_{\text{break}}(z, x) = \begin{cases} k_{\text{att}}(z)n_{\text{screw}}^2 v(x), & \text{if } v(x) \geq v_{\text{parent}}^{\text{min}} \text{ and } l_e(x) + l_i(x) + p(x) \neq 0, \\ 0 & \text{otherwise,} \end{cases} \quad (22)$$

190 where k_{att} is the attrition rate constant and $v_{\text{parent}}^{\text{min}}$ is the minimum agglomerate size that can undergo breakage. As in Braumann et al. [23], the daughter distribution of each breakage event $B_{\text{frag}}(x)$ is described by a beta function with skewness parameters α_{daughter} and β_{daughter} .

2.8. Compartmentalisation/transport

195 To reflect the variable processing environments along the length of the twin-screw, in both parts of this study the screw is modelled as three perfectly mixed compartments arranged in series (see Figure 1).

2.9. Penetration

The transfer of external liquid to internal liquid is modelled as a continuous process. The rate of liquid penetration for each computational particle is controlled by a penetration rate constant k_{pen} and liquid binder viscosity μ_{binder} as

$$r_{\text{pen}} = k_{\text{pen}}\mu_{\text{binder}}^{-1/2} l_e(p - l_i), \quad (23)$$

such that

$$\frac{ds_o}{dt} = 0, \quad \frac{dl_e}{dt} = -r_{\text{pen}}, \quad \frac{dl_i}{dt} = r_{\text{pen}}, \quad \frac{dp}{dt} = -r_{\text{pen}}. \quad (24)$$

3. Stochastic particle methods for granulation

200 3.1. Particle type-space

In the SWA, in each compartment z , a set of stochastic particles is simulated in order to describe the population balance problem. The stochastic particles take the form

$$(z_i, x_i, w_i), \quad i = 1, \dots, N_T(t), \quad (25)$$

where $x \in \mathbb{X}$, $w_i \in (0, w_{\max}]$ is the statistical weight of the particle with index i and $N_T(t)$ is the total number of particles across all z at time t .

The statistical weights offer an additional level of freedom in the construction of the simulation algorithm, whilst maintaining the property

$$\frac{1}{V_{\text{samp}}} \sum_{i=1}^{N(z,t)} w_i \varphi(z, x_j) \xrightarrow{V_{\text{samp}} \rightarrow \infty} \int_{\mathbb{X}} \varphi(z, x_j) P(t, z, dx). \quad (26)$$

Here, V_{samp} is the normalisation parameter or *sample volume* associated with compartment z ; $N(z, t)$ is the number of stochastic particles in compartment z ; $\varphi(z, x_j)$ is some suitable test function which is continuous and with compact support [39] and finally $P(t, z, dx)$ is a concentration measure (i.e. a measure valued quantity) that corresponds to the solution of the population balance problem to be solved. As mentioned in Section 1, (26) may be interpreted as saying that the physical concentration of particles represented by stochastic particle $x_i(t)$ is approximately w_i/V_{samp} . In the same way, the total particle concentration in compartment z is $\sum w_i/V_{\text{samp}}$. As in Lee et al. [25], the sample volume is initialised such that

$$\frac{1}{V_{\text{samp}}(z)} \sum_{i=1}^{N(z,0)} w_i \approx \int_{\mathbb{X}} P(0, z, dx). \quad (27)$$

The particle doubling/reduction method employed by Lee et al. [25] is used to control the number of computational particles in the system. Each compartment
 205 is initialised with $N(0) = 0.75N_{\max}$ computational particles, where N_{\max} is the maximum number of particles permitted. For the purposes of error reduction, the minimum number of particles permitted is $(3/8)N_{\max}$.

The Markov jump process that evolves the system in time is defined by the possible jumps and their associated rates. Each available jump and the associated rate is a function of the state of the system. At each t there exists a list of possible jumps which have independent, exponentially distributed waiting times. In this way, the earliest jump is selected and carried out, generating a modified system of particles with a new state and new rates. The solution then steps forward in time and the process is repeated until some stopping condition is met. The time step is described by the distribution:

$$P(t, t_{\text{wait}} \geq \theta) = \exp(-R_{\text{total}}^{\text{SWA}}(t)\theta), \quad \theta \geq 0, \quad (28)$$

where $R_{\text{total}}^{\text{SWA}}$ is the total jump rate.

3.2. Stochastic weighted algorithm

210 The possible SWA jump processes and associated rates used in this work are:

3.2.1. Inception

The inception process is used to introduce purely solid particles into the system, representing the continuous addition of feed powder to the first simulated compartment of the twin-screw system. In this jump process, a new computational particle of the form

$$(z, x_{\text{incept}}(d), w_{\text{incept}}(d)) \quad (29)$$

is added to compartment z at rate [# events/unit-time/unit-volume]

$$I_{\text{solid}}^{\text{SWA}}(z, dd, dw) := \frac{\dot{M}_{\text{feed}}(z) \mathbb{1}_{\{1\}}(z)}{V_{\text{real}}(z) \bar{v}_{\text{incept}} K_w} \delta_{w_{\text{incept}}(d)}(w) q_{0, \text{incept}}^{\text{SWA}}(d) dd dw, \quad (30)$$

where w_{incept} is the particle inception weight (which may have some dependence on the inception particle diameter d), $q_0^{\text{SWA}}(d)$ is the diameter distribution of 215 incepted (weighted) computational particles and K_w is a scaling factor.

In order for the SWA inception jump to recover the dynamics of the un-weighted, model inception process (and hence the physical inception distribution

$q_{0,\text{incept}}(d)$), it is required that the inception rate take the form [46]

$$I_{\text{solid}}^{\text{SWA}}(z, dd, dw) = \frac{\delta_{w_{\text{incept}(x)}}(w)}{w_{\text{incept}(x)}} I_{\text{solid}}(z, dd) dw \quad (31)$$

$$= \frac{\dot{M}_{\text{feed}} \mathbb{1}_{\{1\}}(z) \delta_{w_{\text{incept}}}(w)}{\rho_s V_{\text{real}}(z) w_{\text{incept}}(d)} q_{0,\text{incept}}(d) dd dw. \quad (32)$$

Equating (30) and (32) we see that

$$w_{\text{incept}}(d) = K_w \frac{q_{0,\text{incept}}(d)}{q_{0,\text{incept}}^{\text{SWA}}(d)}. \quad (33)$$

Rearranging Equation (33) and integrating both sides over the full set of inception particle diameters, one sees that

$$K_w = \frac{\int_{d_{\text{min}}}^{d_{\text{max}}} w_{\text{incept}}(d) q_{0,\text{incept}}^{\text{SWA}}(d) dd}{\int_{d_{\text{min}}}^{d_{\text{max}}} q_{0,\text{incept}}(d) dd} \quad (34)$$

$$= \bar{w}_{\text{incept}}, \quad (35)$$

where \bar{w}_{incept} is the number mean weight of particles selected for (solid) inception. Thus,

$$w_{\text{incept}}(d) = \bar{w}_{\text{incept}} \frac{q_{0,\text{incept}}(d)}{q_{0,\text{incept}}^{\text{SWA}}(d)}. \quad (36)$$

Note that, by asserting that the weights of incepted particles have some dependence on x , the distribution of computational particles on diameters space can be selected freely, whilst still reproducing some physical particle distribution $q_{0,\text{incept}}(d)$. To the best of the author's knowledge, this is the first time that this weighting procedure has been formalised in the context of a stochastic population balance equation. In this paper, we investigate the performance of the complete stochastic weighted algorithm for various forms of $q_{0,\text{incept}}^{\text{SWA}}(d)$ (and hence $w_{\text{incept}}(d)$) within the context of a twin-screw granulation model.

Finally, the total rate of inception jumps in the SWA ([# events/unit-time]) is

$$R_{\text{incept}}^{\text{SWA}}(z, t) = \frac{R_{\text{incept}}(z, t) V_{\text{samp}}(z, t)}{\bar{w}_{\text{incept}}}. \quad (37)$$

In the SWA, the liquid addition jump event results in the addition of a computational particle with the form

$$(z, x_{\text{drop}}, w_{\text{drop}}), \quad (38)$$

where x_{drop} is given by (7) and w_{drop} is the statistical weight of the incepted droplet particles. Unlike incepted solid particles, incepted droplet particles are mono-disperse, hence w_{drop} is simply a constant. Given some sample volume $V_{\text{samp}}(z, t)$, the jump rate associated with this process is then

$$R_{\text{drop}}^{\text{SWA}}(z, t) = \frac{R_{\text{drop}}(z, t)V_{\text{samp}}(z, t)}{w_{\text{drop}}}. \quad (39)$$

An important point to be taken from (39) is that the rate of droplet inception jumps can be controlled through the selection of w_{drop} . This is critical when sampling rare model events which have a high impact on the ensemble properties of interest. In this paper, the effect of the choice of w_{drop} on the performance of the complete simulation algorithm is investigated.

3.3.1. Nuclei growth

Following the approach taken by Kotalczyk and Kruis [47] to carry out coagulation processes, the addition of individual particles of the form (z, x_i, w_i) to the partially formed nucleus $(z, x_{\text{nuc}}, w_{\text{nuc}})$ is carried out as

$$(z, x_{\text{nuc}}, w_{\text{nuc}}), (z, x_i, w_i) \mapsto (z, T_{\text{nuc}}(x_{\text{nuc}}, x_i), \gamma_{\text{nuc}}(w_{\text{nuc}}, w_i)), (z, x_{\text{nuc}}, w_{\text{nuc}} - \gamma_{\text{nuc}}(w_{\text{nuc}}, w_i)), \\ (z, x_i, w_i - \gamma_{\text{nuc}}(w_{\text{nuc}}, w_i)). \quad (40)$$

. Here, γ_{nuc} is the nucleation weight transfer function which, again, follows the approach of Kotalczyk and Kruis [47] such that

$$\gamma_{\text{nuc}}(w_{\text{nuc}}, w_i) = \min(w_{\text{nuc}}, w_i). \quad (41)$$

In order to achieve convergence, the jump process in (40) occurs with rate [47]

$$K_{\text{nuc}}(x_{\text{nuc}}, x_i) \max(w_{\text{nuc}}, w_i). \quad (42)$$

where K_{nuc} is the nucleation kernel. Since it is computationally expensive to compute the expression in (42) for all possible ensemble particles (x_i, w_i) , a majorant form of this kernel is used. This takes the form:

$$\tilde{K}_{\text{nuc}}(x_{\text{nuc}}, w_{\text{nuc}}, x_i, w_i) = K_{\text{nuc}}(x_{\text{nuc}}, x_i)(w_{\text{nuc}} + w_i). \quad (43)$$

The procedure used to pick particle (x_i, w_i) to take part in the jump process (40) is discussed later in this paper, since a number of simplifications may be made after the introduction of the model nucleation kernel $K_{\text{nuc}}(x, y)$. In order to ensure that the jump process (40) is performed at the correct rate, upon selection of the ensemble particle (z, x_i, w_i) to be added to the partially formed nucleus, the jump is performed with probability

$$\frac{\max(w_i, w_{\text{nuc}})}{w_i + w_{\text{nuc}}}, \quad (44)$$

otherwise the jump is fictitious and we move on to the selection of the next ensemble particle. For a more detailed account of the majorant kernel technique the reader is referred to Lee et al. [12].

235 3.4. Immersion nucleation

When nuclei growth is rapid ($k_{\text{nuc}} \rightarrow \infty$) it becomes possible to combine the droplet inception and successive nuclei growth jumps into a unified jump process, which we will refer to as a immersion nucleation jump. The unified jump process begins with the inception of a droplet particle of the form (38). Nucleation growth jump events (40) are repeatedly applied to the droplet particle. This occurs in an iterative manner i.e particle $(z, T_{\text{nuc}}(x_{\text{nuc}}, x_i), \gamma_{\text{nuc}}(w_{\text{nuc}}, w_i))$ is passed back through the jump process (40) with a new ensemble particle x_i . This iterative process continues until

$$T_{\text{nuc}}(x_{\text{nuc}}, x_i) \notin \mathbb{X}_{\text{nuc}}. \quad (45)$$

When (45) is satisfied, $T_{\text{nuc}}(x_{\text{nuc}}, x_i)$ may no longer be passed through jump (40) and a new computational particle is incepted into compartment z with the form

$$(z, T_{\text{nuc}}(x_{\text{nuc}}, x_i), \gamma_{\text{nuc}}(w_{\text{nuc}}, w_i)). \quad (46)$$

This marks the end of the unified immersion nucleation jump process.

In the event that the jump (40) creates two partially formed nuclei¹, then jump (40) must also be separately carried out on particle $(z, x_{\text{nuc}}, w_{\text{nuc}} - \min(w_{\text{nuc}}, w_i))$ until the stopping condition (45) is satisfied for this particle.

Since the rate limiting step of the immersion nucleation jump is the droplet inception, the total jump rate of this process is

$$R_{\text{nuc}}^{\text{SWA}}(z, t) = R_{\text{drop}}^{\text{SWA}}(z, t). \quad (47)$$

240 The implementation of the immersion nucleation jump is discussed in detail in Section 4.3.

3.4.1. Coagulation/compaction

SWA coagulation jumps take different forms depending on whether or not the particles can be successfully coalesced. Additionally, this jump process includes a potential compaction transformation on the particles involved. For successful coalescence, the jump takes the form

$$(z, x_i, w_i), (z, x_j, w_j) \mapsto (z, T_{\text{comp}}(x_i + x_j), \gamma_{\text{coag}}(x_i, w_i, x_j, w_j)), (z, x_j, w_j), \quad (48)$$

and for unsuccessful coalescence (i.e. a compaction/rebound):

$$(z, x_i, w_i), (z, x_j, w_j) \mapsto (z, T_{\text{comp}}(x_i), w_i), (z, x_j, w_j). \quad (49)$$

In the above, γ_{coag} is the coagulation weight transfer function and T_{comp} is the compaction transformation. As in Lee et al. [25] we impose that

$$\gamma_{\text{coag}}(x_i, w_i, x_j, w_j) = w_i \frac{m(x_i)}{m(x_i + x_j)}. \quad (50)$$

The total collision jump rate in compartment z is

$$R_{\text{col}}^{\text{SWA}}(z, t) = \frac{1}{V_{\text{samp}}(z, t)} \sum_{i \neq j}^{N_{\text{comp}}(z, t)} K_{\text{col}}(z, x_i, x_j) w_j. \quad (51)$$

¹Note that additional, partially formed nuclei particles can be formed by (40) if $w_{\text{nuc}} > w_i$.

3.4.2. Breakage

In this paper, the breakage jumps take the form

$$(z, x_i, w_i) \mapsto (z, y, \gamma_{\text{frag}}(x_i, w_i, y)), \quad (52)$$

which occurs at rate

$$g_{\text{break}}(z, x). \quad (53)$$

Here, γ_{frag} is the breakage weight transfer function which takes the form [25]

$$\gamma_{\text{frag}}(x_i, w_i, y) = w_i \frac{m(x_i)}{m(y)}. \quad (54)$$

As in [25, 12], y is selected as:

$$y = x_j, \quad \text{with probability} = \frac{m(x_j)}{m(x_i)}, \quad (55)$$

$$y = x_i - x_j, \quad \text{with probability} = 1 - \frac{m(x_j)}{m(x_i)}, \quad (56)$$

and x_j is selected according to the probability measure $B_{\text{break}}(x_i)$.

The total breakage jump rate in compartment z is

$$R_{\text{break}}^{\text{SWA}}(z, t) = \sum_{i=1}^{N(z,t)} g_{\text{break}}(z, x_i). \quad (57)$$

245 3.4.3. Transport

Particles are permitted to move between compartments according to the jump

$$(z, x_i, w_i) \mapsto (z + 1, x_i, F_c(z)w_i), \quad (58)$$

at rate

$$\frac{1}{\tau(z)}. \quad (59)$$

Here, $\tau(z)$ is the characteristic residence time of compartment z and F_c is the transport weight scaling factor, which takes the form [26]

$$F_c(z) = \frac{V_{\text{samp}}(z+1)}{V_{\text{samp}}(z)} \quad (60)$$

for a series of compartments with equal real volume.

The total transport jump rate in compartment z is

$$R_{\text{outflow}}^{\text{SWA}}(z, t) = \frac{N(z, t)}{\tau(z)}. \quad (61)$$

3.4.4. Overall jump rate

The total jump rate of the stochastic weight algorithm $R_{\text{total}}^{\text{SWA}}$ is given by

$$R_{\text{total}}^{\text{SWA}}(t) = \sum_{z \in \mathbb{L}} \left[R_{\text{col}}^{\text{SWA}}(z, t) + R_{\text{break}}^{\text{SWA}}(z, t) + R_{\text{nuc}}^{\text{SWA}}(z, t) + R_{\text{incept}}^{\text{SWA}}(z, t) + R_{\text{outflow}}^{\text{SWA}}(z, t) \right]. \quad (62)$$

Particle process $p \in \{\text{col}, \text{break}, \text{nuc}, \text{incept}, \text{outflow}\}$ in compartment z is carried out at time t with probability

$$\frac{R_p^{\text{SWA}}(z, t)}{R_{\text{total}}^{\text{SWA}}(t)}. \quad (63)$$

3.4.5. Continuous processes

Intra-particle processes (such as liquid penetration) may be modelled as
 250 continuous processes. To minimise the computational cost of modelling such mechanisms, these are carried out using the linear process deferment algorithm (LPDA) [48]. LPDA has been successfully employed in the solution of stochastic population balance models for granulation [25], silica nanoparticle synthesis [26] and soot particle formation [48, 39]. In the LPDA, each stochastic particle is
 255 time stamped and the application of all linear processes is deferred until:

1. The next occurrence of a non-linear event (.e.g. coagulation). At which point linear processes are applied to the particles involved in the jump.
2. The compartmental system has been simulated to/beyond the next deferment check point time (based on predefined list of deferment check
 260 points). At which point linear processes are applied to all stochastic particles, thereby updating each particle to the current simulation time. This occurs between stochastic jumps events.

4. Numerical studies

In this section we investigate the influence of key numerical factors such as
265 the choice of inception weighting scheme, the statistical weights/weight trans-
fer function associated with the nucleation process and the general convergence
properties of complete stochastic weighting algorithm in the context of the twin-
screw model. To ensure that the results of this analysis are relevant to typical
model operating conditions (equipment operating conditions and rate constant
270 values), all numerical tests are carried out using the equipment operating con-
ditions and optimised model rate constants used/optimised in the first part of
this study. These parameters are repeated in Table 2 and Table 3, respectively.

4.1. Simulation details

In this section we describe the simulation conditions used throughout the
275 numerical studies. These parameters are to be assumed in all cases unless
explicitly stated otherwise.

4.1.1. Simulation stop time and repetitions

Since the twin-screw granulation system is a continuous system, we are
primarily interested in the steady state solution of the twin-screw PBM. As
280 such, dynamic results are not assessed in this study. Visual analysis of the re-
sponses showed that the time at which simulation responses ceased to drift with
 t was controlled by the total system residence time. The final simulation time
 $t_{\text{stop}} = 5 \sum_{z \in \mathbb{Z}} \tau(z) \approx 40\text{s}$ proved to be an acceptable choice and is used across
all numerical studies in this paper.

285 Each simulation is carried out until $t = t_{\text{stop}}$ and this process is repeated
 n_{runs} times, each time with a different seed to the pseudo-random number gen-
erator. In this study, each repetition will be referred to as a run.

4.1.2. Quantification of errors

For the stochastic simulations in this work, temporal functionals $M(t)$ are reported as averages taken over all runs as

$$\eta(t) = \frac{1}{n_{\text{runs}}} \sum_{i=1}^{n_{\text{runs}}} M_i(t), \quad (64)$$

where the functional may be a particle ensemble property such as the mass
 290 fraction of particles in a particular sieve class.

The half-width of the confidence internals are

$$c(t) = 1.64 \sqrt{\frac{\sum_{i=1}^{n_{\text{runs}}} (M_i(t) - \eta(t))^2}{n_{\text{runs}}^2}}, \quad (65)$$

which corresponds to a confidence interval $P = 0.9$ [25]. In cases where the statistical error is to be measured, the mean confidence interval \bar{c} of a measured distribution is used. This is computed as

$$\bar{c} = \frac{1}{n_{\text{points}}} \sum_{j=1}^{n_{\text{points}}} c_j, \quad (66)$$

where n_{points} is the number of discrete points in the responses distribution of interest.

When a high precision solution (HPS) is used as a reference point, the sum of squared errors of prediction (SSE) is used to represent the systematic error and is given by²

$$\text{SSE} = \sum_{j=1}^{n_{\text{points}}} (\eta_{\text{HPS},j} - \eta_j)^2. \quad (67)$$

All HPS's were run with $N_{\text{max}} = 65536$, $n_{\text{runs}} = 10$ and $w_{\text{nuc}} = 0.001$.

4.1.3. Binary tree

295 To ensure that the computational cost of solving the model is minimised, binary tree caches are employed to store key particle properties, thus enabling fast computation of ensemble wide properties (e.g overall breakage rate) [39, 48, 49, 50].

²Note that (67) does not have any weighting factors since all η of interest are of the same physical dimension and order of magnitude.

4.1.4. Hardware set-up

300 All test simulations were carried out using a single core of an Intel® Sandy Bridge™ E5-2670 3.30GHz Processor with 4GB of RAM per core.

4.2. Inception sampling methods

In this section, we investigate various forms of the inception function $q_{0,\text{incept}}^{\text{SWA}}(d)$ and the resulting weight transfer functions $w_{\text{incept}}(d)$ (see (30) and (36)) in the context of the twin-screw granulation model presented in Section 2. We are reminded that $q_{0,\text{incept}}^{\text{SWA}}(d)$ represents the frequency at which stochastic particles of the form $(z, x_{\text{incept}}(d), w_{\text{incept}}(d))$ with diameter d are selected within an inception jump, such that some physical inception particle size distribution $q_{0,\text{incept}}(d)$ is recovered.

In previous SWA studies [25, 12], the authors have employed

$$\begin{aligned} q_{0,\text{incept}}^{\text{SWA}}(d) &= q_{0,\text{incept}}(d), \quad \bar{w}_{\text{incept}} = 1, \\ &\rightarrow w_{\text{incept}}(d) = 1, \end{aligned} \tag{68}$$

310 which we shall refer to as the equi-weighted inception scheme for SWA (EWI-SWA).

EWI-SWA is attractive due to its ease of implementation, however, in some cases, it has been observed that significant reduction in computational cost can be attained using more complex forms of $w_{\text{incept}}(d)$, depending upon the ensemble property of interest.

As an example, let us consider the case where we are interested in measuring the mass distribution (as a function of d) within the steady state ensemble of the twin-screw granulation simulation. It is often the case that the real density distribution of particles $q_{0,\text{incept}}(d)$ covers a d range which is several orders of magnitude in size (such is the case of that presented for Lactose Impalpable in Hagrasy et al. [43]). Given such a situation, we see from Figure 3(a) (blue trace) that the particles which occur with the greatest frequency are those with d much smaller than d_{max} . Consequently, most ‘real’ particles that are incepted into the physical system will have a volume (and thus mass) which is several

Table 2: Summary of simulation parameters.

Parameter	Type	Value	Unit
d_{drop}	Operating parameter	2×10^{-3}	m
\dot{M}_{feed}	Operating parameter	4.0	kg hr ⁻¹
n_{screw}	Operating parameter	6.67	rev s ⁻¹
$V_{\text{real,T}}$	Equipment geometry	4.05×10^{-5}	m ³
e_{coag}	Material property	0.2	-
ρ_l	Material property	998	kg m ⁻³
ρ_s	Material property	1545	kg m ⁻³
μ_{binder}	Material property	10^{-3}	Pa s
d_{max}	Model parameter	3.31×10^{-6}	m
d_{min}	Model parameter	8.26×10^{-4}	m
H_a	Model parameter	5×10^{-6}	m
k_{reac}	Model parameter	3	-
$v_{\text{parent}}^{\text{min}}$	Model parameter	1.80×10^{-11}	m ⁻³
$v_{\text{nuc}}^{\text{max}}$	Model parameter	v_{drop}	m ³
α_{daughter}	Model parameter	5.0	-
β_{daughter}	Model parameter	2.0	-
ε_{min}	Model parameter	0.5	-
ν_{max}	Model parameter	0.5	-
τ	Model parameter	2.76	s
ϕ_{max}	Model parameter	1.08	-

Table 3: Optimised model rate constants generated in first part of this study, used in numerical tests.

Compartment	1,3			2			1-3
index z							
Parameter	k_{col}	k_{att}	k_{comp}	k_{col}	k_{att}	k_{comp}	k_{pen}
Unit	m^3	m^{-1}s	-	m^3	m^{-1}s	-	$\text{kg}^{\frac{1}{2}}\text{m}^{-\frac{7}{2}}\text{s}^{-\frac{3}{2}}$
Value	1.21×10^{-10}	9.42×10^6	0.395	9.99×10^{-13}	1.09×10^9	0.954	10.0

orders of magnitude less than that held by particles with d close to the upper limit of the inception range. Now, if one were to employ the EWI-SWA scheme (i.e. $q_{0,\text{incept}}^{\text{SWA}}(d) = q_{0,\text{incept}}(d)$) in such a situation, then it follows that most of the stochastic particles that are incepted will also carry very little volume (and hence very low mass), and thus have a very limited effect on the compartment mass distribution. However, occasionally stochastic particles with large d will be incepted into compartment 1, causing a temporary but significant change in the system mass distribution. This results in a high degree of stochastic noise within the measured product mass distribution. In order to mitigate this noise, it is required that the maximum number of computational particles N_{max} and/or n_{runs} be increased, both of which increase the computational cost of simulation.

From the thought experiment above, we see that it would be advantageous to spread the incepted mass over the incepted stochastic particles in a more uniform manner, while still recovering $q_{0,\text{incept}}$. This is not only true of the inception process, but also the initialisation of the ensemble at $t = 0$. We further note that the transport processes also have the ability to induce a high degree of noise in the mass distribution when the compartment particle mass is poorly distributed across the ensemble of stochastic particles.

Methods to control the distribution of selected quantities, analogous to that described above, have been employed by Zhao and co-workers [40, 36, 41] and DeVille et al. [51] in the context of alternative particle models. In this paper we adapt the size dependent particle weighting approach of Zhao and Zheng

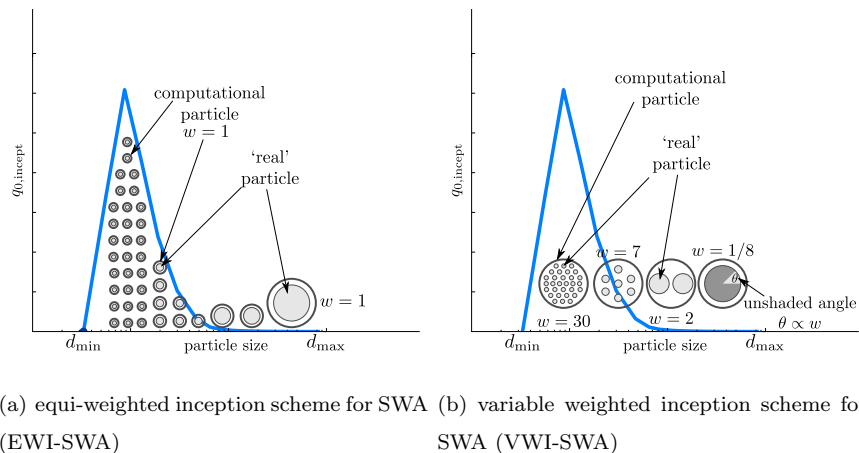


Figure 3: An illustrative example of the various sampling methods studied. In VWI-SWA, many small particles are grouped in a few computational particles, reducing the total number required to accurately sample ‘mass-rich’ regions of the distribution closer to d_{max} .

[40] to the inception jump process (29) of the twin-screw model and also, to the initialisation of the ensemble (outlined in Section 3). Specifically, in this work, we investigate the case where $q_{0,\text{incept}}^{\text{SWA}}$ is a uniform distribution over d with normalised form

$$q_{0,\text{incept}}^{\text{SWA}}(d) = (d_{\text{max}} - d_{\text{min}})^{-1}. \quad (69)$$

It follows from (36) that

$$w_{\text{incept}}(d) = \bar{w}_{\text{incept}}(d_{\text{max}} - d_{\text{min}})q_{0,\text{incept}}(d). \quad (70)$$

The use of (69) and (70) for inception will be referred to as the variable weighted inception scheme for SWA (VWI-SWA). The use of VWI-SWA results in a stochastic particle distribution analogous to that illustrated in Figure 3(b). Numerical tests were carried out to assess the performance of the EWI-SWA and VWI-SWA inception algorithms described above. To ensure that the rates of each process were matched between compared sets of simulations at $t = 0$, the values of w_{drop} was modified in the EWI-SWA case. For VWI-SWA w_{drop} was set to 16.38 in all simulations.

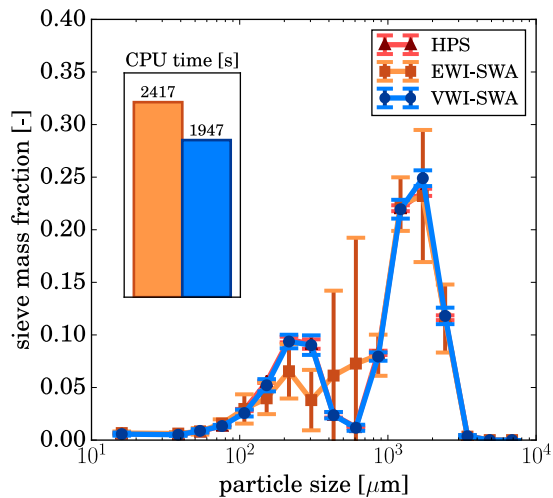


Figure 4: A comparison of the product mass fraction distributions ($z=3$) and CPU times using the VWI-SWA and EWI-SWA algorithms with $N_{\max}=8192$. A high precision solution using VWI-SWA is included but sits directly behind the blue trace.

The product ensembles of each simulation are sieved using a sieve set starting from $32\mu\text{m}$ to $8064\mu\text{m}$ with a $\sqrt{2}$ geometric progression. Sieve mass fractions are plotted against the mid-point of the corresponding sieve intervals.

The resulting sieved exit mass fraction distributions using both EWI-SWA and VWI-SWA with $N_{\max} = 8192$ are presented in Figure 4. It is noted that, for the EWI-SWA scheme, most of the computational feed particles have been utilised to form the lower end of the distribution between $10\text{-}100\mu\text{m}$. As a result, sampling of the primary particle distribution is much poorer for larger particle diameters (where most of the ensemble mass resides). The error in these larger sieve classes for the EWI-SWA scheme has carried over into the steady state solution. By contrast, the VWI-SWA scheme has sampled the initial distribution with much higher precision in the larger sieve classes, resulting in a steady state distribution with relatively small confidence intervals across the complete diameter range. Since both simulations operated with the same bounds on the number computational particles permitted, it is expected that both EWI and VWI-SWA schemes should result in CPU times which are of the same order

of magnitude. This is confirmed by the inset CPU plot in Figure 4, where the weighted inception algorithm has showed a similar but slightly reduced CPU time over the EWI-SWA scheme. The variations in CPU time likely reflect the interaction between the particle selection procedure of the nucleation algorithm and the ensemble weight distribution. This interaction may change the rate at which particles are fully depleted (deleted from the ensemble) by the mechanism, altering the equilibrium computational particle count and, hence, the CPU time.

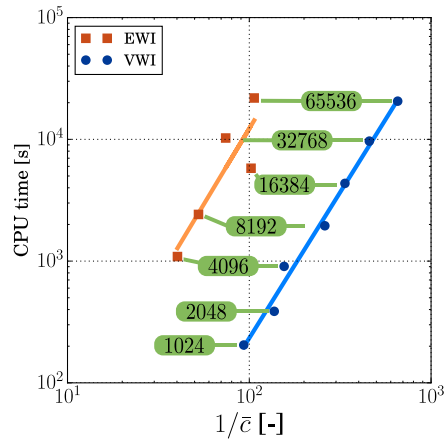


Figure 5: A comparison of the total CPU time vs. associated inverse average confidence interval half-width in the sieved exit mass fraction distribution for 40s of simulation with $n_{\text{runs}} = 10$. The number of computational particles (attached green blocks) is varied to yield different CPU times and $1/\bar{c}$ values.

The scaling performance of each inception/initialisation algorithm was assessed by running a series of simulations with varying N_{\max} (and therefore the minimum number of computational particles, as $N_{\min} = 3N_{\max}/8$). Simulations were run with $N_{\max}=1024$ and increased by a factor of two to a final $N_{\max}=65536$. Simulations using the EWI-SWA scheme proved to be numerically unstable for $N_{\max}=[1024, 2048]$, and thus results for these operating points are not reported here. The resulting set of mean confidence interval half-widths

\bar{c} across the resulting sieve exit mass fraction distribution and their associated CPU times are presented in Figure 5. Here, $1/\bar{c}$ is used to quantify the precision of each response.

385 It is clear from Figure 5 that the VWI-SWA scheme offers a much higher precision solution than the equivalent EWI-SWA (same CPU time). Specifically, the VWI-SWA scheme can be seen to yield solutions in CPU times almost two orders of magnitude lower than the EWI-SWA for the same level of precision.

4.3. Immersion nucleation parameters

390 In this section, we investigate the selection of the key parameter w_{drop} , the selection of ensemble particles x_i and simplification of the iteration process within the nucleation jump process (40) for the twin-screw granulation test case.

4.3.1. Selection of the droplet weight

We are reminded that the statistical weight of incepted droplets w_{drop} is a free parameter within the context of the nucleation jump process. Furthermore, we observe from (8) and (39) that the rate of immersion nucleation jumps in compartment $z = 1$ has the characteristic

$$R_{\text{nuc}}^{\text{SWA}}(1, t) \propto (v_{\text{drop}} w_{\text{drop}})^{-1}. \quad (71)$$

In previous SWA efforts in the modelling of high shear batch granulation [24, 12], 395 alternative droplet particle inception jump processes with jump rates given by equations of the form (71) have been implemented with the equivalent of $w_{\text{nuc}} = 1$. In these examples the value of v_{drop} was very small (on the order of 10^{-13}m^3) to reflect the operation of the equipment being modelled. As a result, the rate of this process was significant (relative to the total jump rate) allowing it to be 400 sampled with a high degree of accuracy.

However, in the case of twin-screw granulation, operating values of v_{drop} can be much larger (on the order of 10^{-8}m^3). Hence, if $w_{\text{drop}} = 1$, then the nucleation jump rate can be exceptionally low relative to the total jump rate, resulting in poor sampling of this jump process. In addition to this, it is noted

405 that a single nucleation jump can have a significant impact on the particle mass distribution within the ensemble (particularly when w_{drop} is on the order of \bar{w}_{incept}), and hence poor nucleation sampling results in a high degree of stochastic noise in the product mass distribution. This ultimately places a limit on the size of v_{drop} that can be modelled with an acceptable degree of error (with
410 $w_{\text{drop}}=1$). Again, like the case of poor solid particle inception sampling, this noise can be mitigated by increasing N_{max} and n_{runs} at an additional computational cost. In this study, we avoid the need to increase N_{max} and/or n_{runs} by dynamically selecting w_{drop} according to the operating conditions to be modelled. It will be demonstrated that, in doing so, we can ensure the effective
415 sampling of this important jump process within the context of the twin-screw granulation model.

4.3.2. Simplification of the jump

As mentioned in Section 3.3.1, the nucleation particle addition jump (40) has the drawback of potentially creating more than a single partially formed nucleus in the jump products (when $w_{\text{nuc}} < w_i$). This additional, partially formed nuclei must also then be separately and repeatedly passed through jump (40) until the condition (45) is satisfied. This is undesirable as these additional nuclei have the potential to create yet more nuclei, so on and so forth, before (45) is satisfied. Hence it is possible that this process may become computationally taxing and flood the ensemble with particles which are physically very similar, and possesses very low statistical weights. To avoid these issues we note that, in the context of the twin-screw model, ensemble particles x_i that are able to attached to the partially formed (i.e. those for which $K_{\text{nuc}}(x_{\text{nuc}}, x_i) \neq 0$) are generally much smaller in volume than the corresponding nucleus x_{nuc} . Hence, the addition of a single x_i to x_{nuc} has relatively little effect on the state of x_{nuc} i.e.

$$T_{\text{nuc}}(x_{\text{nuc}}, x_i) \approx x_{\text{nuc}}. \quad (72)$$

Furthermore, we note that the statistical weight of the first partially formed nucleus (in the case where two nuclei are formed) is $\min(w_{\text{nuc}}, w_i) = w_i$, which is

generally much greater than the weight of the secondary nucleus ($w_{\text{nuc}} - w_i$). As such, the product particles may be combined into a single representative particle using a weighted average of the particles of $(T_{\text{nuc}}(x_{\text{nuc}}, x_i), w_i)$, $(x_{\text{nuc}}, \min(w_{\text{nuc}} - w_i))$ with the form:

$$(w_{\text{nuc}}^{-1} [w_i T_{\text{nuc}}(x_{\text{nuc}}, x_i) + (w_{\text{nuc}} - w_i)x_{\text{nuc}}], w_{\text{nuc}}). \quad (73)$$

It was observed that, for the systems modelled in this paper, this simplification had no discernible effect on the model solution but offered modest reduction in simulation times (5-10%) and code complexity, therefore this simplification is employed in all simulations within this study. An illustrative example of the immersion nucleation jump process is presented in Figure 6.

4.3.3. Selection of ensemble particles

As alluded to in previous sections, the selection of computational particles (x_i, w_i) for addition to partially formed nuclei by way of jump (40) can be simplified based on the model nucleation kernel K_{nuc} employed. Combining (43) and (14) we see that the majorant form of the nucleation kernel for the twin-screw model is

$$\tilde{K}_{\text{nuc}}(x_{\text{nuc}}, w_{\text{nuc}}, x_i, w_i, z, t) = k_{\text{nuc}}(z, t)v(x_i)(w_{\text{nuc}} + w_i)\mathbb{1}_{\{x|v(x_i) < v_{\text{drop}}\}}(x_i) \quad (74)$$

Since only a single nuclei particle is considered at a time, the total rate of this process is

$$\begin{aligned} \sum_{i=1}^{N(z,t)} \tilde{K}_{\text{nuc}}(x_{\text{nuc}}, w_{\text{nuc}}, x_i, w_i, z, t) &= \sum_{i=1}^{N(z,t)} k_{\text{nuc}}(z)v(x_i)(w_{\text{nuc}} + w_i)\mathbb{1}_{\{x|v(x_i) < v_{\text{drop}}\}}(x_i) \\ &= k_{\text{nuc}}(z) \sum_{i=1}^{N(z,t)} v(x_i)\mathbb{1}_{\{x|v(x_i) < v_{\text{drop}}\}}(x_i) \\ &+ k_{\text{nuc}}(z) \sum_{i=1}^{N(z,t)} v(x_i)w_i\mathbb{1}_{\{x|v(x_i) < v_{\text{drop}}\}}(x_i). \end{aligned} \quad (75)$$

Thus, particle (x_i, w_i) is selected to take part in the jump (40) based on the selection property $v(x_i)$ with probability

$$\mathbb{P}_{v(x_i)} = \frac{w_{\text{nuc}} \sum_{i=1}^{N(z,t)} v(x_i) \mathbb{1}_{\{x|v(x_i) < v_{\text{drop}}\}}(x_i)}{w_{\text{nuc}} \sum_{i=1}^{N(z,t)} v(x_i) \mathbb{1}_{\{x|v(x_i) < v_{\text{drop}}\}}(x_i) + \sum_{i=1}^{N(z,t)} v(x_i) w_i \mathbb{1}_{\{x|v(x_i) < v_{\text{drop}}\}}(x_i)}. \quad (76)$$

It follows that particle (x_i, w_i) is selected to take part in the jump (40) based on the selection property $v(x_i)w_i$ with probability

$$\mathbb{P}_{v(x_i)w_i} = 1 - \mathbb{P}_{v(x_i)}. \quad (77)$$

425 Using a binary tree to store properties $v(x_i) \mathbb{1}_{\{x|v(x_i) < v_{\text{drop}}\}}(x_i)$ and $v(x_i)w_i \mathbb{1}_{\{x|v(x_i) < v_{\text{drop}}\}}(x_i)$ for each computational particle allows for rapid evaluation of the the summations in (76) and hence the evaluation of $\mathbb{P}_{v(x_i)}$ and the selection of particle x_i with the desired probability measure.

The complete nucleation algorithm (including the particle selection procedure described above) is provided in Appendix Appendix A.

4.3.4. Nucleation performance

To assess the affect of w_{drop} on the performance of twin-screw simulations, several simulations were carried out using the VWI-SWA algorithm and $N_{\text{max}} = 1024$ for various values of w_{drop} in the range $5 \times 10^{-5} - 5 \times 10^{-2}$. All errors were constructed from the sieved mass fraction distribution in the final reactor (435 $z = 3$).

From Figure 7(a) we note that the mean confidence interval half-width \bar{c} varies relatively smoothly with w_{drop} and \bar{c} exhibits an increase towards the limits of the w_{drop} range investigated. The picture painted by the SSE in the same figure is less clear towards low w_{drop} , however, from PSD's in Figure 7(b) (440 we see that all simulation solutions lie in close proximity to the HPS, regardless of w_{drop} and thus the SSE values are subject to a high degree of noise in this operating range. The increase in \bar{c} and SSE towards the upper ranges of the tested w_{drop} is indicative of the poor sampling of the nucleation jump, as discussed in Section 4.3.1. Towards the lower range of w_{drop} , the nucleation jump rate is very (445

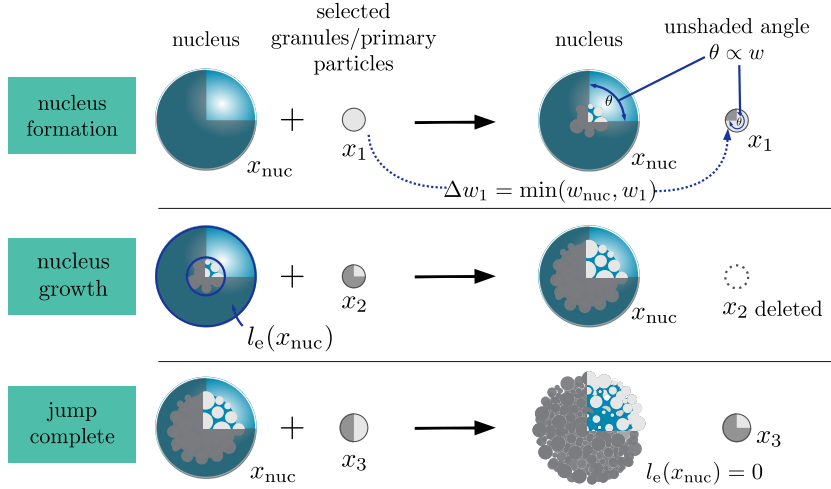
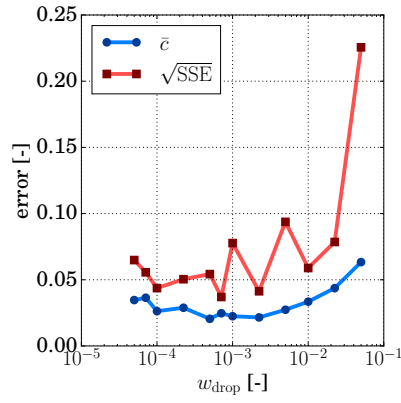


Figure 6: An illustration of the SWA immersion nucleation scheme. Each particle represents a single computational particle. The angle of the unshaded region of each particle is constructed such that it is proportional to the associated statistical weight of the particle. Each pathway corresponds, respectively, to the first, intermediate (with particle removal) and final iteration of the particle selection loop of Algorithm 1 (steps 3-12).

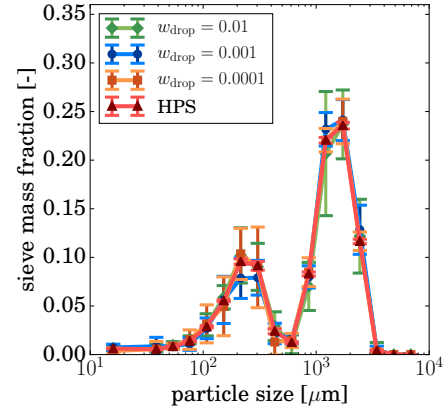
high and the absolute liquid mass carried by the stochastic nuclei particles at the start of the jump is relatively low. Since the amount of solid particles that interact with the droplet is roughly proportional to the absolute liquid mass of the stochastic droplet particle, the number of solid particles acted on by each nuclei jump becomes much lower. Hence we expect greater fluctuations in the primary particle mode at low w_{drop} , as observed in the left-most peak in the PSD of Figure 7(b).

As expected, in Figure 7(c) we see that, in general, the CPU time is reduced with increasing w_{drop} as the total jump rate is reduced. This trend diminishes towards large w_{drop} as nucleation ceases to be the dominant jump process. For $w_{\text{drop}} > 0.007$, coagulation becomes the dominant jump process (in terms of CPU-time) and so the computation time becomes independent of w_{drop} . In Figure 7(d), the combination of error and CPU time data for various values of w_{drop} shows that there exists a favourable range of w_{drop} approximately between

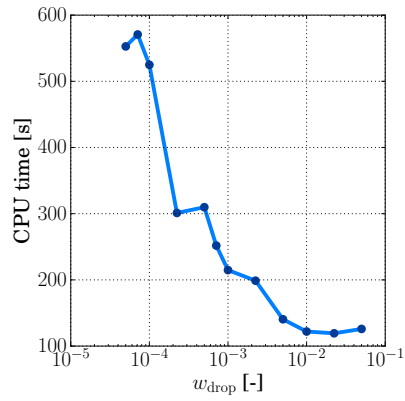
⁴⁶⁰ $10^{-2} - 5 \times 10^{-4}$ where both the error and computation time are minimised.



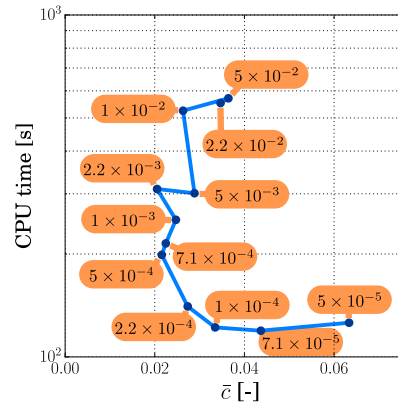
(a)



(b)



(c)



(d)

Figure 7: The effect of varying w_{drop} on simulation performance. All results correspond to the steady state sieved mass fraction distribution in $z = 3$. In (d) the value of w_{drop} corresponding to each point is indicated within the attached blocks.

4.4. Convergence properties

It is useful to consider the convergence properties of the complete stochastic algorithm for the twin-screw test case. This is done by assessing how the systematic and statistical error in the final mass distribution depends on N_{\max} and n_{runs} . All convergence tests are carried out with the VWI-SWA algorithm and $w_{\text{nuc}} = 0.001$.

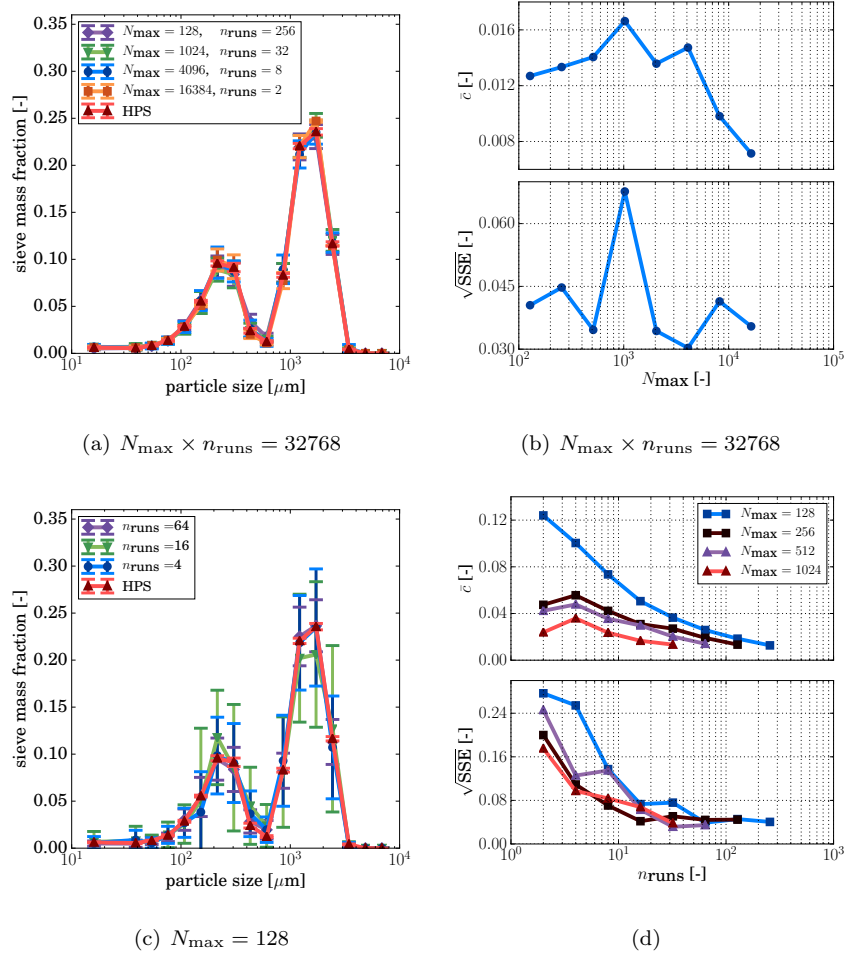


Figure 8: Convergence properties of the twin-screw SWA framework using VWI-SWA.

In Figure 8(a) and 8(b) we show the dependence of the final mass distribu-

tion and its associated error on N_{\max} for an approximately fixed computational budget by holding $N_{\max} \times n_{\text{runs}}$ constant at 32768. In this region of operating space, we see that there is no correlation between N_{\max} and the statistical or systematic error measures and that all measured mass distributions lie on top of the HPS. Both of these observations indicate that the simulation algorithm is extremely robust against changes in N_{\max} , provided that the n_{runs} is scaled appropriately. Lower values of N_{\max} could not be explored as the algorithm became numerically unstable for $N_{\max} < 128$. These instabilities are induced by the fact that the incepted nuclei particles can no longer gather sufficient solid mass to complete the nucleation jump process.

Thus, in order to access regions of operating space where the systematic and statistical error is more significant, it is required that lower values of $N_{\max} \times n_{\text{runs}}$ are used. In Figure 8(c) we show the variation in the final mass distribution and the associated confidence intervals with fixed $N_{\max}=128$ for varying values of n_{runs} . This figure shows that $N_{\max} \times n_{\text{runs}}$ can be lowered to 8192 before the mass distribution begins to significantly deviate from the HPS. It is also clear that at even with $n_{\text{runs}}=4$ the solution still lies in close proximity to the HPS, though the confidence intervals have dramatically increased in size, as expected.

This region of operating space is further explored in Figure 8(d), which shows how the statistical and systematic error varies with n_{runs} for low values of N_{\max} . Here, if we compare simulations of equal $N_{\max} \times n_{\text{runs}}$ (i.e. comparable CPU times) then we observe that, in general, there is no clear dependence between N_{\max} and statistical or systematic error for low values of N_{\max} . From this analysis we may conclude that, for a twin-screw test case investigated, if a desired level of error in the final mass distribution is desired (either systematic or statistical), then there is no significant benefit of increasing N_{\max} provided that N_{\max} exceeds the value required for computational stability (128 in this case).

5. Conclusions

In this paper, we have presented a stochastic weighted particle framework that can be used to solve the four-dimensional twin-screw granulation PBM introduced and optimised in the first part of this study. A new nucleation
500 jump process is outlined, which is compatible with an immersion nucleation model in the context of wet granulation. A variable weighting particle inception/initialisation algorithm was constructed to aid the efficient sampling of wide primary particle size distributions. This inception algorithm was shown to deliver performance increases of between one and two orders of magnitude
505 over the traditional equi-weighted inception scheme. The numerical properties of the new nucleation jump process were explored and it was observed that there exists a specific range of droplet statistical weight that minimises both the error in the final mass fraction distribution and the computational cost of simulation. The convergence properties of the complete algorithm were assessed using the
510 twin-screw test case and it was shown that the algorithm is extremely robust against changes in the number of computational particles used.

Acknowledgements

The authors would like to thank AstraZeneca for funding this work. This work was partially funded by EPSRC Grant 1486478 and the National Research
515 Foundation (NRF), Prime Minister's Office, Singapore under its Campus for Research Excellence and Technological Enterprise (CREATE) programme.

Abbreviations

ANN	Artificial neural network
DSA	Direct simulation algorithm
DEM	Discrete element method
EWI-SWA	Equally weighted inception for the stochastic weighted algorithm
HPS	High precision solution
LPDA	Linear process deferment algorithm
PBM	Population balance model
MC-PBM	Monte Carlo population balance model
SWA	Stochastic weighted algorithm
TSG	Twin-screw granulation
VWI-SWA	Variable weighting inception for the stochastic weighted algorithm

Nomenclature

Roman symbols

B_{break}	breakage daughter distribution probability measure	-
c	confidence interval half-width	-
\bar{c}	average confidence interval half-width (of a distribution)	-
d	particle diameter	m
d_{drop}	droplet diameter	m
d_{max}	maximum primary particle diameter	m
d_{min}	minimum primary particle diameter	m
E	set of valid nuclei particles	-
F_c	transport weight scaling factor	-
g_{break}	particle breakage rate	s^{-1}
H_a	height of surface asperities	m
I_{solid}	solid particle inception rate	$\text{m}^{-3}\text{s}^{-1}$
$I_{\text{solid}}^{\text{SWA}}$	weighted solid particle inception rate	$\text{m}^{-3}\text{s}^{-1}$

k_{att}	breakage rate constant	s m^{-1}
k_{col}	collision rate constant	m^3
k_{comp}	compaction rate constant	-
k_{nuc}	nucleation rate constant	s^{-1}
k_{pen}	penetration rate constant	$\text{kg}^{1/2}\text{m}^{-7/2}\text{s}^{-3/2}$
k_{reac}	number of compartments	-
K_{col}	size independent collision kernel	m^3s^{-1}
k_v	shape factor	-
K_{nuc}	nucleation kernel	m^3s^{-1}
\tilde{K}_{nuc}	majorant nucleation kernel	m^3s^{-1}
l_e	external liquid volume	m^3
$l_{e,\text{nuc}}$	nuclei external liquid volume	m^3
l_i	internal liquid volume	m^3
\mathbb{L}	the set of compartment indices	-
LSR	operating liquid solid mass flowrate ratio	-
m	particle mass	kg
M	model functional	-
\dot{M}_{feed}	solid mass flowrate	kg s^{-1}
n_{runs}	number of simulation repetitions	-
n_{screw}	screw speed	rev s^{-1}
N	number of stochastic particles	-
n_{comp}	number of compartments	-
N_{max}	maximum number of stochastic particles/compartment	-
N_{min}	maximum number of stochastic particles/compartment	-
N_{T}	total number of stochastic particles in all compartments	-
p	pore volume	m^3
P	density of the population distribution	m^{-3}

$q_{0,\text{incept}}$	number based physical particle size distribution for inception	m^{-1}
$q_{0,\text{incept}}^{\text{SWA}}$	number based weighted particle size distribution for inception	m^{-1}
q_3	number based particle size distribution	m^{-1}
r_{pen}	particle penetration rate	m^3s^{-1}
R_{incept}	model particle inception rate	$\text{s}^{-1}\text{m}^{-3}$
$R_{\text{break}}^{\text{SWA}}$	SWA breakage jump rate	s^{-1}
$R_{\text{col}}^{\text{SWA}}$	SWA collision jump rate	s^{-1}
$R_{\text{incept}}^{\text{SWA}}$	SWA particle inception jump rate	s^{-1}
$R_{\text{nuc}}^{\text{SWA}}$	SWA nucleation jump rate	s^{-1}
R_{outflow}	model particle outflow rate	s^{-1}
$R_{\text{outflow}}^{\text{SWA}}$	SWA particle outflow jump rate	s^{-1}
$R_{\text{total}}^{\text{SWA}}$	SWA total jump rate	s^{-1}
s_o	original solid volume	m^3
SSE	sum of squared errors of prediction	-
t	time	s
t_{wait}	jump waiting time	s
T_{comp}	compaction type transformation	m^3
$T_{\text{comp}}^{l_e}$	compaction external liquid transformation	m^3
$T_{\text{comp}}^{l_i}$	compaction internal liquid transformation	m^3
T_{comp}^p	compaction pore volume transformation	m^3
T_{nuc}	nucleation type transformation	m^3
v	particle volume	m^3
\bar{v}_{incept}	number average feed particle volume	m^3
$v_{\text{parent}}^{\text{min}}$	minimum volume for breakage	m^3
v_{drop}	droplet volume	m^3
$v_{\text{nuc}}^{\text{max}}$	maximum particle volume involved in nucleation	m^3
v_{drop}	droplet volume	m^3

V_{real}	physical compartment volume	m^3
$V_{\text{real,T}}$	total physical volume of all compartments combined	m^3
V_{samp}	compartment sample volume	m^3
w	particle statistical weight	-
\bar{w}_{incept}	mean inception particle statistical weight	-
w_{incept}	inception particle statistical weight	-
w_{drop}	droplet particle statistical weight	-
w_{nuc}	nuclei statistical weight	-
x	particle vector	-
x_{drop}	droplet particle vector	-
x_{nuc}	nuclei particle vector	-
$x_{\text{nuc}}^{\text{start}}$	initial nuclei particle vector	-
\mathbb{X}	particle type-space	-
\mathbb{X}_{nuc}	nuclei particle type-space	-
z	compartment index	-
Greek symbols		
α_{daughter}	breakage distribution parameter	-
β_{daughter}	breakage distribution parameter	-
γ_{coag}	coagulation weight transfer function	-
γ_{frag}	breakage weight transfer function	-
γ_{nuc}	nucleation weight transfer function	-
ε	particle porosity	-
ε_1	post-compaction particle porosity	-
ε_{min}	minimum particle porosity	-
η	run averaged model measure	-
μ_{binder}	binder viscosity	Pa s
ρ_1	binder density	kg m^{-3}

ρ_s	solid density	kg m^{-3}
ϕ	liquid saturation	-
ϕ_{max}	maximum liquid saturation	-
τ	compartment residence time	s

525 **Appendix A. SWA immersion nucleation algorithm**

Algorithm 1: The SWA immersion nucleation algorithm.

- 1 Set the droplet volume v_{drop} and initial nucleus particle state $(x_{\text{nuc}}, w_{\text{nuc}})$ to that of a droplet particle:

$$v_{\text{drop}} \leftarrow \pi d_{\text{drop}}^3 / 6,$$

$$x_{\text{nuc}} \leftarrow x_{\text{drop}} = (0, v_{\text{drop}}, 0, 0),$$

$$w_{\text{nuc}} \leftarrow w_{\text{drop}}.$$

- 2 **while** $l_e(x_{\text{nuc}}) > 0$ **do**
- 3 Choose particle selection procedure according to (76) and (77).
- 4 Choose particle x_i from compartment z according to selection procedure.
- 5 Generate a uniform random number $\mathcal{U}(0, 1)$.
- 6 **if** $\mathcal{U} < \max(w_i, w_{\text{nuc}})/(w_i + w_{\text{nuc}})$ **then**
- 7 Set $\gamma_{\text{nuc}} \leftarrow \min(w_i, w_{\text{nuc}})$.
- 8 Create particle $(z, T_{\text{nuc}}(x_{\text{nuc}}, x_i), \gamma_{\text{nuc}})$.
- 9 Set $w_i \leftarrow w_i - \gamma_{\text{nuc}}$.
- 10 Set $w_{\text{nuc}} \leftarrow w_{\text{nuc}} - \gamma_{\text{nuc}}$.
- 11 **if** $w_i = 0$ **then**
- Remove particle x_i from the ensemble
- if** $w_{\text{nuc}} > 0$ **then**
- Product nuclei are to be combined
- $x_{\text{nuc}} \leftarrow (w_{\text{nuc}}^{-1}(w_i T_{\text{nuc}}(x_{\text{nuc}}, x_i) + (w_{\text{nuc}} - w_i)x_{\text{nuc}}, w_{\text{nuc}})$
- $w_{\text{nuc}} \leftarrow w_{\text{nuc}} + \gamma_{\text{nuc}}$
- else**
- Jump is fictitious. Go to Step 3
- 12 Add newly formed nucleus $(x_{\text{nuc}}, w_{\text{nuc}})$ into compartment z .
- 13 Move forward in time and select next jump event.
-

References

1. Iveson SM, Litster JD, Hapgood K, Ennis BJ. Nucleation, growth and breakage phenomena in agitated wet granulation processes: a review. Powder Technology 2001;117(1-2):3 – 39. doi:10.1016/S0032-5910(01)00313-8.
530
2. Ramkrishna D. Population Balances: Theory and Applications to Particulate Systems in Engineering. Elsevier Science; 2000.
3. Shirazian S, Kuhs M, Darwish S, Croker D, Walker GM. Artificial neural network modelling of continuous wet granulation using a twin-screw extruder. International Journal of Pharmaceutics 2017;doi:10.1016/j.ijpharm.2017.02.009.
535
4. Behzadi SS, Klocker J, Hüttlin H, Wolschann P, Viernstein H. Validation of fluid bed granulation utilizing artificial neural network. International Journal of Pharmaceutics 2005;291(1-2):139 –48. doi:http://dx.doi.org/10.1016/j.ijpharm.2004.07.051.
540
5. Barrasso D, Walia S, Ramachandran R. Multi-component population balance modeling of continuous granulation processes: A parametric study and comparison with experimental trends. Powder Technology 2013;241:85 – 97.
6. Barrasso D, Hagrasy AE, Litster JD, Ramachandran R. Multi-dimensional population balance model development and validation for a twin screw granulation process. Powder Technology 2015;270, Part B:612 –21. doi:10.1016/j.powtec.2014.06.035.
545
7. Kumar A, Germaey KV, Beer TD, Nopens I. Model-based analysis of high shear wet granulation from batch to continuous processes in pharmaceutical production - A critical review. Eur J Pharm Biopharm 2013;85(3, Part B):814 –32.
550

8. Kumar A, Vercruyse J, Mortier ST, Vervaet C, Remon JP, Ger-
naey KV, Beer TD, Nopens I. Model-based analysis of a twin-
555 screw wet granulation system for continuous solid dosage manufactur-
ing. Computers & Chemical Engineering 2016;89:62 – 70. doi:10.1016/
j.compchemeng.2016.03.007.
9. Barrasso D, Eppinger T, Pereira FE, Aglave R, Debus K, Bermingham
SK, Ramachandran R. A multi-scale, mechanistic model of a wet gran-
560 ulation process using a novel bi-directional PBM-DEM coupling algo-
rithm. Chemical Engineering Science 2015;123:500 –13. doi:10.1016/j.
ces.2014.11.011.
10. Bouffard J, Bertrand F, Chaouki J. A multiscale model for the simulation
of granulation in rotor-based equipment. Chemical Engineering Science
565 2012;81:106 –17.
11. Cundall PA, Strack OD. A discrete numerical model for granular assem-
blies. Geotechnique 1979;29(1):47–65.
12. Lee KF, Dosta M, McGuire AD, Mosbach S, Wagner W, Heinrich S,
Kraft M. Development of a multi-compartment population balance
570 model for high-shear wet granulation with discrete element method.
Computers & Chemical Engineering 2017;99:171 –84. doi:10.1016/j.
compchemeng.2017.01.022.
13. Barrasso D, Ramachandran R. Qualitative assessment of a multi-scale,
compartmental PBM-DEM model of a continuous twin-screw wet gran-
575 ulation process. Journal of Pharmaceutical Innovation 2016;11(3):231–49.
doi:10.1007/s12247-015-9240-7.
14. Barrasso D, Tamrakar A, Ramachandran R. A reduced order PBM-ANN
model of a multi-scale PBM-DEM description of a wet granulation process.
Chemical Engineering Science 2014;119:319–29.

- 580 15. Barrasso D, Tamrakar A, Ramachandran R. Model order reduction of a multi-scale PBM-DEM description of a wet granulation process via ANN. Procedia Engineering 2015;102(Supplement C):1295 –304. doi:doi.org/10.1016/j.proeng.2015.01.260.
16. Barrasso D, Ramachandran R. A comparison of model order reduction
585 techniques for a four-dimensional population balance model describing multi-component wet granulation processes. Chemical Engineering Science 2012;80:380 –92. doi:10.1016/j.ces.2012.06.039.
17. Gantt JA, Gatzke EP. A stochastic technique for multidimensional granulation modeling. AIChE Journal 2006;52(9):3067–77. doi:10.1002/aic.
590 10911.
18. Braumann A, Goodson MJ, Kraft M, Mort PR. Modelling and validation of granulation with heterogeneous binder dispersion and chemical reaction. Chemical Engineering Science 2007;62(17):4717 –28. doi:10.1016/j.ces.2007.05.028.
- 595 19. Braumann A, Man PLW, Kraft M. Statistical approximation of the inverse problem in multivariate population balance modeling. Journal of Industrial and Engineering Chemistry 2010;49(1):428–38. doi:10.1021/ie901230u.
20. Braumann A, Kraft M, Mort PR. Parameter estimation in a multidimensional granulation model. Powder Technology 2010;197(3):196 – 210.
600 doi:10.1016/j.powtec.2009.09.014.
21. Braumann A, Kraft M. Incorporating experimental uncertainties into multivariate granulation modelling. Chemical Engineering Science 2010;65(3):1088 –100. doi:10.1016/j.ces.2009.09.063.
- 605 22. Braumann A, Man PLW, Kraft M. The inverse problem in granulation modeling-two different statistical approaches. AIChE Journal 2011;57(11):3105–21. doi:10.1002/aic.12526.

23. Braumann A, Kraft M, Wagner W. Numerical study of a stochastic particle algorithm solving a multidimensional population balance model for high shear granulation. Journal of Computational Physics 2010;229(20):7672 – 91. doi:10.1016/j.jcp.2010.06.021.
24. Lee KF, Mosbach S, Kraft M, Wagner W. A multi-compartment population balance model for high shear granulation. Computers & Chemical Engineering 2015;75:1 – 13. doi:10.1016/j.compchemeng.2015.01.009.
25. Lee KF, Patterson RIA, Wagner W, Kraft M. Stochastic weighted particle methods for population balance equations with coagulation, fragmentation and spatial inhomogeneity. Journal of Computational Physics 2015;303:1 – 18. doi:10.1016/j.jcp.2015.09.031.
26. Menz WJ, Akroyd J, Kraft M. Stochastic solution of population balance equations for reactor networks. Journal of Computational Physics 2014;256:615–29.
27. Mosbach S, Su H, Kraft M, Bhave A, Mauss F, Wang Z, Wang JX. Dual injection homogeneous charge compression ignition engine simulation using a stochastic reactor model. International Journal of Engine Research 2007;8(1):41–50. doi:10.1243/14680874JER01806. arXiv:10.1243/14680874JER01806.
28. Cao L, Su H, Mosbach S, Kraft M, Bhave A, Kook S, Bae C. Studying the influence of direct injection on PCCI combustion and emissions at engine idle condition using two dimensional CFD and stochastic reactor model. 2008. doi:10.4271/2008-01-0021; sAE Technical Paper No. 2008-01-0021. doi:10.4271/2008-01-0021.
29. Balthasar M, Kraft M. A stochastic approach to calculate the particle size distribution function of soot particles in laminar premixed flames. Combustion and Flame 2003;133(3):289 –98. doi:10.1016/S0010-2180(03)00003-8.

30. Celnik M, Patterson RIA, Kraft M, Wagner W. Coupling a stochastic soot population balance to gas-phase chemistry using operator splitting. Combustion and Flame 2007;148(3):158–76. doi:10.1016/j.combustflame.2006.10.007.
- 640
31. Zhao H, Zheng C. Stochastic algorithm and numerical simulation for drop scavenging of aerosols. Applied Mathematics and Mechanics 2006;27(10):1321–32. doi:10.1007/s10483-006-1004-z.
32. Vikhansky A, Kraft M. Single-particle method for stochastic simulation of coagulation processes. Chemical Engineering Science 2005;60(4):963–7. doi:10.1016/j.ces.2004.09.062.
- 645
33. Zhao H, Kruis FE, Zheng C. Reducing statistical noise and extending the size spectrum by applying weighted simulation particles in Monte Carlo simulation of coagulation. Aerosol Science and Technology 2009;43(8):781–93. doi:10.1080/02786820902939708. arXiv:10.1080/02786820902939708.
- 650
34. Rjasanow S, Wagner W. A stochastic weighted particle method for the Boltzmann equation. Journal of Computational Physics 1996;124(2):243–53. doi:10.1006/jcph.1996.0057.
- 655
35. Eibeck A, Wagner W. Stochastic particle approximations for Smoluchoski's coagulation equation. The Annals of Applied Probability 2001;11(4):1137–65.
36. Zhao H, Kruis FE, Zheng C. A differentially weighted Monte Carlo method for two-component coagulation. Journal of Computational Physics 2010;229(19):6931–45. doi:10.1016/j.jcp.2010.05.031.
- 660
37. Patterson RIA, Wagner W. A stochastic weighted particle method for coagulation–advection problems. SIAM Journal on Scientific Computing 2012;34(3):B290–311. doi:10.1137/110843319. arXiv:10.1137/110843319.

- 665 38. Zhao H, Zheng C, Xu M. Multi-Monte Carlo approach for general dynamic equation considering simultaneous particle coagulation and breakage. Powder Technology 2005;154(2-3):164 –78. doi:10.1016/j.powtec.2005.04.042.
39. Patterson RIA, Wagner W, Kraft M. Stochastic weighted particle methods for population balance equations. Journal of Computational Physics 670 2011;230(19):7456 –72. doi:10.1016/j.jcp.2011.06.011.
40. Zhao H, Zheng C. A new event-driven constant-volume method for solution of the time evolution of particle size distribution. Journal of Computational Physics 2009;228(5):1412 –28. doi:10.1016/j.jcp.2008.10.033. 675
41. Zhao H, Zheng C. A population balance-Monte Carlo method for particle coagulation in spatially inhomogeneous systems. Computers & Fluids 2013;71:196 – 207. doi:10.1016/j.compfluid.2012.09.025.
42. Dhenge RM, Cartwright JJ, Hounslow MJ, Salman AD. Twin screw granulation: Steps in granule growth. International Journal of Pharmaceutics 680 2012;438(1-2):20 – 32.
43. Hagrasy AE, Hennenkamp J, Burke M, Cartwright J, Litster J. Twin screw wet granulation: Influence of formulation parameters on granule properties and growth behavior. Powder Technology 2013;238:108 –15. doi:10.1016/j.powtec.2012.04.035. 685
44. Allen T. Particle size measurement. Springer; 2013.
45. Hapgood KP, Litster JD, Smith R. Nucleation regime map for liquid bound granules. AIChE Journal 2003;49(2):350–61.
46. Patterson RIA. Numerical modelling of soot formation. PhD dissertation; 690 The University of Cambridge; 2007.

47. Kotalczyk G, Kruis F. A Monte Carlo method for the simulation of coagulation and nucleation based on weighted particles and the concepts of stochastic resolution and merging. Journal of Computational Physics 2017;340:276–96. URL: <http://www.sciencedirect.com/science/article/pii/S002199911730236X>. doi:10.1016/j.jcp.2017.03.041.
- 695
48. Patterson RIA, Singh J, Balthasar M, Kraft M, Norris J. The linear process deferment algorithm: A new technique for solving population balance equations. SIAM Journal on Scientific Computing 2006;28(1):303–20.
49. Menz WJ, Kraft M. The suitability of particle models in capturing aggregate structure and polydispersity. Aerosol Science and Technology 2013;47(7):734–45. doi:10.1080/02786826.2013.788244. arXiv:10.1080/02786826.2013.788244.
- 700
50. Sander M, West RH, Celnik MS, Kraft M. A detailed model for the sintering of polydispersed nanoparticle agglomerates. Aerosol Science and Technology 2009;43(10):978–89. doi:10.1080/02786820903092416. arXiv:10.1080/02786820903092416.
- 705
51. DeVile R, Riemer N, West M. Weighted flow algorithms (WFA) for stochastic particle coagulation. Journal of Computational Physics 2011;230(23):8427–51. doi:10.1016/j.jcp.2011.07.027.